CHEMISTRY
A EUROPEAN JOURNAL

DOI: 10.1002/chem.200800114

A New Photothermal Therapeutic Agent: Core-Free Nanostructured Au_xAg_{1-x} Dendrites

Kuo-Wei Hu,[a] Chih-Chia Huang,[a] Jih-Ru Hwu,[b] Wu-Chou Su,[c] Dar-Bin Shieh,[d] and Chen-Sheng Yeh*[a]

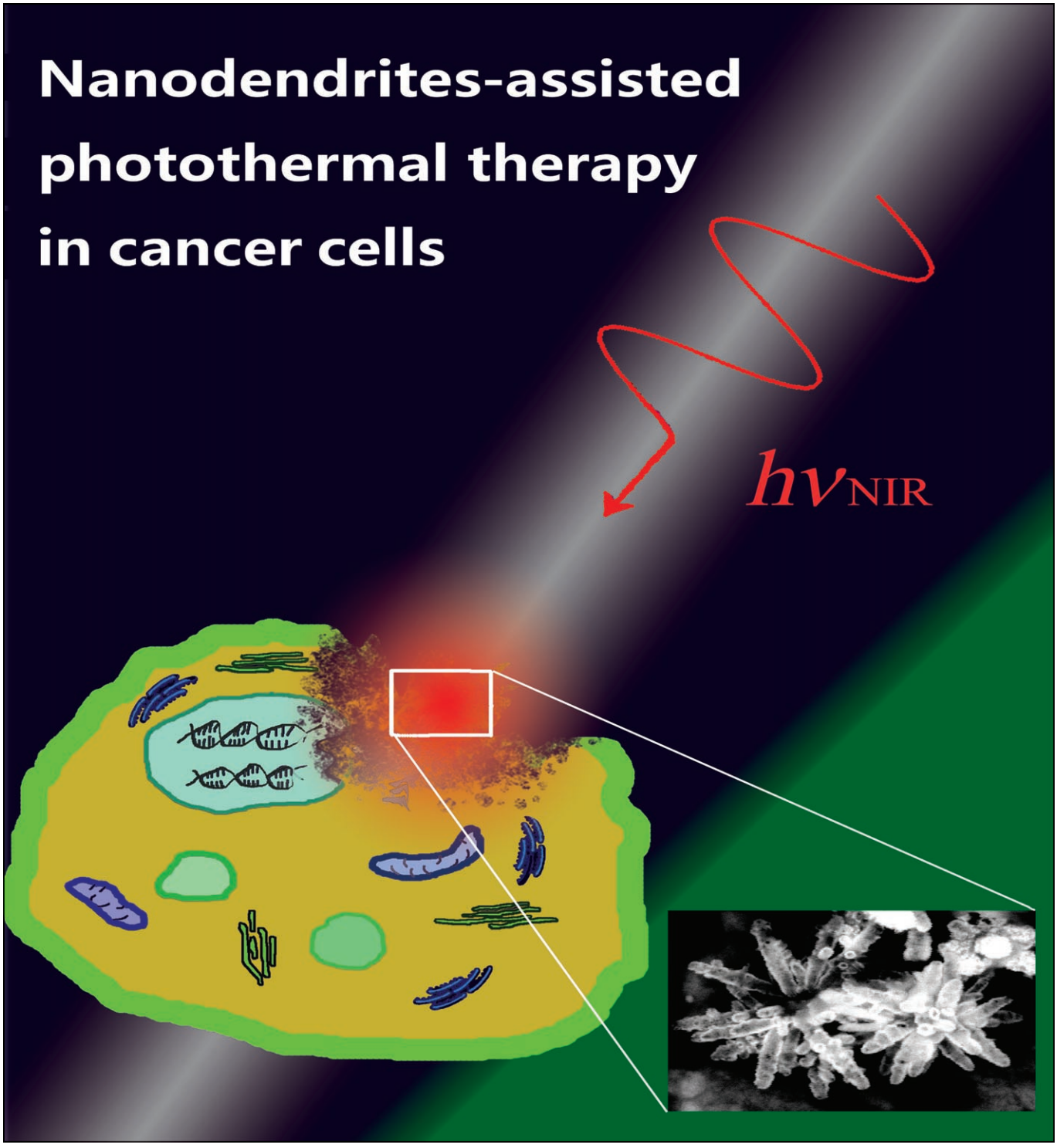

Abstract: A new class of Au_xAg_{1-x} nanostructures with dendrite morphology and a hollow interior were synthesized by using a replacement reaction between Ag dendrites and an aqueous solution of $HAuCl_4$. The Ag nanostructured dendrites were generated by the reaction of $AgNO_3$ with ascorbic acid in a methanol/water system. The dendrites resemble a coral shape and are built up of many stems with an asymmetric arrangement. Each stem is approximately 400 nm in length and 65 nm in diameter. The bimetallic composition of Au_xAg_{1-x} can be tuned by the addition of different amounts of $HAuCl_4$ to the Ag dendritic solution. The hollowing process resulted in tubular structures with a wall thickness of 10.5 nm in $Au_{0.3}Ag_{0.7}$ dendrites. The UV/Vis spectra indicate that the strongest NIR absorption among the resulting hollow Au_xAg_{1-x} dendrites was in $Au_{0.3}Ag_{0.7}$. The MTT assay was conducted to evaluate the cytotoxicity of Ag dendrites, hollow $Au_{0.06}Ag_{0.94}$ and $Au_{0.3}Ag_{0.7}$ dendrites, and Au nanorods. It was found that hollow $Au_{0.06}Ag_{0.94}$ and $Au_{0.3}Ag_{0.7}$ dendrites exhibited good biocompatibility, while both Ag dendrites and Au nanorods showed dose-dependent toxicity. Because of absorption in the NIR region, hollow $Au_{0.3}Ag_{0.7}$ dendrites were used as photothermal absorbers for destroying A549 lung cancer cells. Their photothermal performance was compared to that of Au nanorod photothermal therapeutic agents. As a result, the particle concentration and laser power required for efficient cancer cell damage were significantly reduced for hollow $Au_{0.3}Ag_{0.7}$ dendrites relative to those used for Au nanorods. The hollow $Au_{0.3}Ag_{0.7}$ nanostructured dendrites show potential in photothermolysis for killing cancer cells.

Keywords: dendrites · gold · nanostructures · photothermal therapy · silver

Introduction

The use of nanoparticles in medicine is currently one of the most important applications in the nanotechnology field. Numerous nanoscale materials with different compositions have been used in drug delivery,[1] cancer cell diagnostics,[2] and therapeutics.[3] Among these applications, photothermal cancer therapy with near-infrared laser radiation is an emerging field. This technique provides a minimally invasive alternative to conventional surgical treatment of solid tumors. Thermal therapeutics is relatively simple to perform and has the advantages of fast recovery, fewer complications, and shorter hospital stays. The laser wavelength used in this technique is located in the near-infrared (NIR) region, at which tissue transmission is optimal due to low-energy absorption, providing maximum irradiation penetration through tissue.

Materials absorbing radiation in the NIR range are considered suitable agents for photothermal cancer therapy. Even though no evident surface plasmon absorption band for the dispersed Au nanoparticles was found in the NIR region, the aggregated Au nanoparticles exhibiting NIR absorption can still transform NIR radiation into heat and provide a sufficient increase in temperature for killing cancer cells.[4] Selective photothermolysis with different kinds of Au nanomaterials with a continuous-wave (CW) or ultrafast femtosecond laser has been demonstrated. For example, Halas et al. developed nanoshell nanostructures consisting of silica cores, 110 nm in diameter, embedded in a 10 nm thick Au nanolayer.[3a] The silica@Au core-shell nanostructures with NIR absorption were introduced in photothermal ablation on cancer cells. At a laser exposure of 35 $W cm^{-2}$ for 7 min, all nanoshell-treated SK-BR-3 breast cells underwent photothermal destruction within the laser spot. Xia et al. developed another fascinating Au nanostructure, Au nanocages, and showed their potential as an effective photothermal therapeutic agent for cancer treatment.[5] The nanocages could induce thermal destruction of the SK-BR-3 cancer cells after being irradiated by a mode-locked Ti-sapphire laser with an intensity threshold of only 1.5 $W cm^{-2}$. Kim et al. presented Au nanoshells embedded with Fe_3O_4 nanoparticles (Mag-GNS) to serve a bimodal function for magnetic resonance imaging (MRI) and NIR photothermal therapy.[6] The Mag-GNS-$Ab_{HER2/neu}$-treated SK-BR-3 (Her2/neu-positive breast cancer cells) and H520 (Her2/neu-negative lung cancer cells) cells were exposed to a femtosecond-pulse laser with a wavelength of 800 nm for 10 s. The SK-BR-3 cells began to die at a laser power of 20 mW, which is lower than the power of 60 mW required for H520 cells to die with nonspecific targeting. Additionally, El-sayed et al. showed that Au nanorods, 20 nm in diameter and 78 nm in length, can serve as a photothermal therapeutic agent after

[a] K.-W. Hu,[+] C.-C. Huang,[+] Prof. C.-S. Yeh
Department of Chemistry, National Cheng Kung University
No 1. University Road, Tainan City (Taiwan)
Fax: (+886) 6-274-0552
E-mail: csyeh@mail.ncku.edu.tw

[b] Prof. J.-R. Hwu
Department of Chemistry, National Tsing Hua University
101, Section 2, Kuang-Fu Road, Hsinchu, Taiwan 30013 (Taiwan)

[c] Dr. W.-C. Su
Department of Internal Medicine
National Cheng Kung University
No 1. University Road, Tainan City (Taiwan)

[d] Dr. D.-B. Shieh
Institute of Oral Medicine and Department of Stomatology
National Cheng Kung University
No 1. University Road, Tainan City (Taiwan)

[+] K.-W. Hu and C.-C. Huang contributed equally to this work.

Supporting information for this article is available on the WWW under http://www.chemistry.org or from the author.

the capping of anti-EGFR antibodies on the nanorod surfaces to provide a selective target.[7] They found that after exposure to a CW laser at 800 nm, malignant cells required about half the laser energy than that required for the non-malignant cells for photodestruction.

Herein, core-free, AuAg, nanostructured dendrites are reported for the first time as photothermal therapeutic agents in the treatment of lung cancer cells. Dendritic Ag nanostructures have been fabricated from many wet-chemical routes[8–12] and have shown potential applications as catalysts,[8] in optics, in surface-enhanced Raman scattering (SERS) as bio-sensors,[9] and as superhydrophobic surfaces,[13] because of their supramolecular structures and large surface area. Sun and Hanger synthesized dendritic Ag nanostructures with *p*-phenylenediamine (PPD) acid as a reducing agent.[10d] Ag dendrites also can be produced by means of a polymer-assisted strategy[11] or by using the heterogeneous reaction of silver ions with Zn plate.[9b,10a] Among the different preparation methods, Imai et al. developed a surfactant-free soft method by adjusting the concentration ratio of ascorbic acid (AsA) to silver ions to form flower-like dendritic Ag materials.[12] In this study, we have modified Imai's method by using a water/methanol co-solvent system to fabricate Ag nanostructured dendrites. The reaction of $AgNO_3$ with ascorbic acid in a water/methanol solvent resulted in an assembly of silver nanoparticles in dendritic structures. The resulting Ag dendrites were further hollowed to form bimetallic AuAg dendrites by using a galvanic replacement reaction. The core-free Au_xAg_{1-x} dendrites are composed of tubular branches. The $Au_{0.3}Ag_{0.7}$ dendrites displayed a strong absorption in the NIR region. We have carefully examined and investigated the photothermal performance of $Au_{0.3}Ag_{0.7}$ dendrites on malignant A549 lung cancer cells using a diode CW laser with a wavelength of 808 nm. Since Au nanorods can serve as an effective photothermal therapeutic agent, we have also investigated the photothermal performance of Au nanorods in A549 lung cancer cells and compared the photothermal efficiency of $Au_{0.3}Ag_{0.7}$ nanostructured dendrites with that of Au nanorods.

Results and Discussion

Preparation of core-free, Au_xAg_{1-x}, nanostructured dendrites: The surfactant-free synthesis of dendritic Ag nanostructures was performed in the methanol/water solvent system by the reduction of $AgNO_3$ (0.43 mM) with ascorbic acid (7.15 mM) at room temperature according to the reaction given in Equation (1).

$$C_6H_8O_6 + 2\,Ag^+ \rightarrow 2\,Ag + C_6H_6O_6 + 2\,H^+ \quad (1)$$

A typical scanning electron microscopy (SEM) image (Figure 1a) shows the collected Ag products with well-defined dendritic nanostructures resembling a coral shape. As shown in the image, the Ag dendrites exhibit a form of

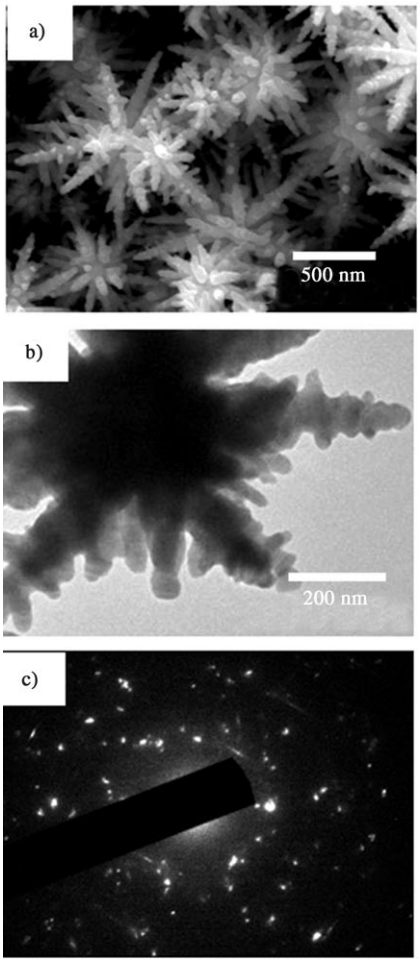

Figure 1. a) SEM and b) TEM images of the dendritic Ag nanostructures. c) ED pattern for an individual dendrite.

radial growth. An individual dendrite is built of many stems with an asymmetric arrangement. The stems are roughly 400 nm in length and 65 nm in diameter. A close up view of a single dendrite reveals that the individual stem is composed of small, asymmetric branches 28 nm in diameter (Figure 1b). The selected area electron diffraction (SAED) pattern was recorded for an individual dendrite, as shown in Figure 1c. The SAED pattern of the polycrystalline structure indicates that the Ag dendrites are crystalline, but have no preferred orientation. The SAED measurements were also taken for the respective stems of one Ag dendrite. Figure 2 shows the SAED patterns and growth direction of each stem, marked by A, B, C, and D. As can be seen from the insets of Figure 2, the SAED patterns display spots superimposed on the ring, indicating that the stems are not perfect crystals. The growth direction of the stems can be assigned as $\langle 200\rangle$ for A, $\langle 311\rangle$ for B, $\langle 220\rangle$ for C, and $\langle 420\rangle$ for D.

To gain insight into the growth process of Ag dendrites, time-dependent transmission electron microscopy (TEM) images were taken to monitor the morphological evolution of silver dendrites (see Supporting Information Figure S1). At the reaction time of 5 s, the results show the formation

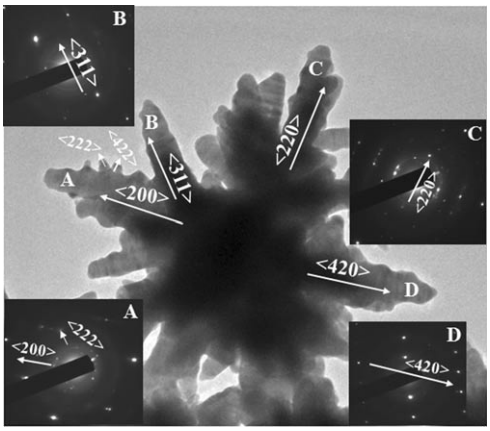

Figure 2. TEM image of the growth direction of individual stems from the dendrite particle. The insets indicate the corresponding ED pattern for stems marked by A, B, C, and D.

of spherical Ag nanoparticles in an aggregated form. Over the period between 5 and 45 s of the reaction time, Ag dendrite nanostructures formed along with some Ag spheres. After 80 s, the growth process was dominated by the development of Ag nanostructured dendrites. Initially, the small Ag nanoparticles were quickly ($\approx$5 s) reduced by the AsA agent, as confirmed by TEM images. At the reaction time of $\approx$45 s, spherical, aggregated network, and dendritic products co-existed in the solution. It seems that aggregation occurred immediately after Ag nanoparticles were generated. The particle aggregation is further supported by the HRTEM images, which show the branches of the dendrite being composed of aggregated particles (see Supporting Information Figure S1d). It is possible that the growth pathway is dominated by a diffusion controlled process;[10c,d,14] that is, the diffusion of Ag nanoparticles plays an important role in the formation of the asymmetric building and leads to the polycrystalline Ag dendrites. The embryo Ag aggregates serve as the clustering cores. The free Ag nanoparticles in the liquid medium diffuse in a random motion and adhere to the cores. The free particles continuously became attached due to diffusion and are anchored by the cores, giving rise to the out-growth irradiating form.

To prepare Au_xAg_{1-x} bimetal nanostructured dendrites, the as-obtained silver dendrites were collected and re-dispersed into an aqueous solution containing PVP polymers. After the addition of the aqueous solution of $HAuCl_4$ into the solution of Ag dendrites in water resulted in a hollowing process that produced dendritic AuAg composites with a tubular morphology. By adjusting the amount of added $HAuCl_4$, different compositions of Au_xAg_{1-x} hollow dendrites can be obtained. Figure 3a shows a SEM image for the hollow $Au_{0.3}Ag_{0.7}$ dendrites. It can be seen that the tips of the stems of the dendrites have a void, indicating tubular nanostructures. The interior structures of the stems were further examined by using TEM (Figure 3b), which shows lower contrast in the interior than at the periphery, providing evidence of a tubular formation. The tubular shell is esti-

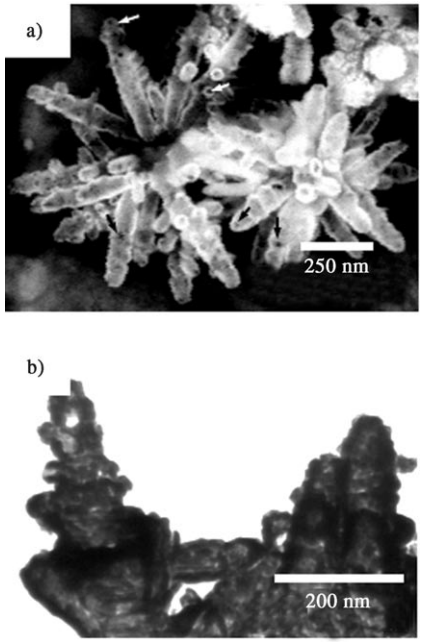

Figure 3. a) SEM and b) TEM images of core-free $Au_{0.3}Ag_{0.7}$ dendrites. The arrows in a) show the voids on the tips of the stems of the dendrites.

mated to be around 10.5 nm thick. In the hollowing process, the solid dendritic Ag can be converted to core-free dendritic nanomaterials by wet-chemical etching. This reaction is based on the spontaneous replacement reaction, because the standard reduction potential of the $AuCl_4^-$/Au pair (0.99 V vs. SHE) is higher than that of the Ag^+/Ag pair (0.88 V vs. SHE).[15] Accordingly, the interiors of the dendritic Ag were oxidized to Ag^+ ions, followed by the combination of Ag^+ with Cl^- ions to form an insoluble AgCl species in the solution. An excess of an aqueous solution of NaCl was used to remove AgCl byproducts through a complex formation of $AgCl_4^{3-}$ (aq).[16]

XRD measurements (Figure 4) characterized the crystal phase of the resulting products before and after the addition of the aqueous solution of $HAuCl_4$. The dendritic Ag particles have a crystalline structure with face-centered cubic (fcc) crystallization (lattice constant of a value in 4.077 Å).

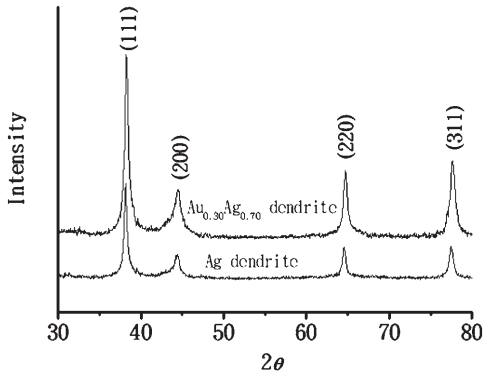

Figure 4. XRD patterns of Ag and core-free $Au_{0.3}Ag_{0.7}$ dendrites.

The hollow $Au_{0.3}Ag_{0.7}$ dendrites produce the same diffraction patterns ($a=4.075$ Å). It is known that fcc metallic Ag and Au are difficult to discriminate, because their fcc isostructure lattice constants [$a=4.086$ Å for Ag (JCPDS 04-0783) and $a=4.078$ Å for Au (JCPDS 04-0784)] are similar. Therefore, energy dispersive X-ray analysis (EDX) was conducted to determine the presence of Au and Ag elements. Figure 5 shows a series of absorption spectra from the silver

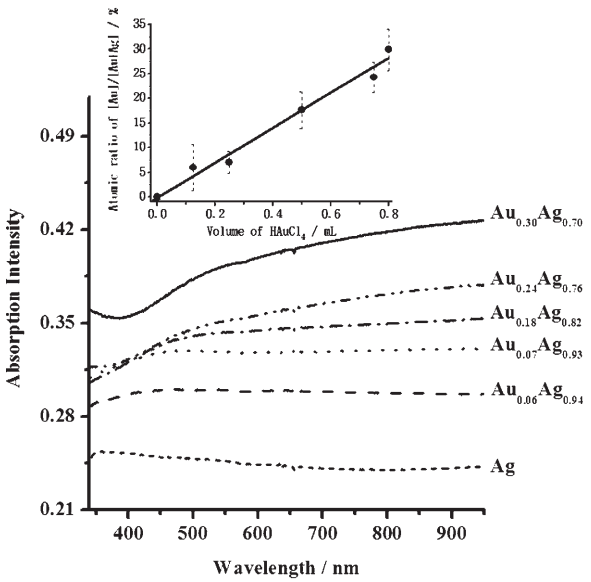

Figure 5. UV/Vis absorption spectra of various Au_xAg_{1-x} composites as a function of the amount of added $HAuCl_4$. The inset shows a linear relationship between the atomic ratio of Au and the amount of added $HAuCl_4$.

dendritic solutions reacted with different amounts of an aqueous solution of $HAuCl_4$ (0.125–0.8 mL). As can be seen, the Au_xAg_{1-x} dendritic absorptions of the UV/Vis spectra appear in the range 400–950 nm. Upon increasing the amount of added $HAuCl_4$, the absorbances relative to each other increased progressively. The absorption spectra show no characteristics and exhibit a flattening contour with an intense tail toward the NIR region. It was found that the bimetallic composition of $Au_{0.3}Ag_{0.7}$, which originated from the addition of an aqueous solution of $HAuCl_4$ (0.8 mL), gave the strongest NIR absorbance. The addition of more than 0.8 mL of the aqueous solution of $HAuCl_4$ resulted in the collapse of the AuAg dendrites leading to fragment formation. EDX analysis was conducted to characterize and determine the atomic ratio of [Au]/[Au+Ag] as a function of the added amount of $HAuCl_4$. The corresponding Au_xAg_{1-x} compositions were identified as $Au_{0.06}Ag_{0.94}$ (0.125 mL), $Au_{0.07}Ag_{.093}$ (0.25 mL), $Au_{0.18}Ag_{.0.82}$ (0.5 mL), $Au_{0.24}Ag_{0\cdot76}$ (0.75 mL), and $Au_{0.3}Ag_{0.7}$ (0.8 mL).

Biocompatibility of Au_xAg_{1-x} nanostructured dendrites, Ag dendrites, and Au nanorods: Before the performance of the photothermal experiments was measured, the cytotoxicity of the different materials was evaluated. Cell viability experiments were conducted on A549 lung cancer cells by means of a 3-(4,5-dimethyl-2-thiazolyl)-2,5-diphenyl-2*H*-tetrazolium bromide (MTT) assay. Figure 6 indicates the results of

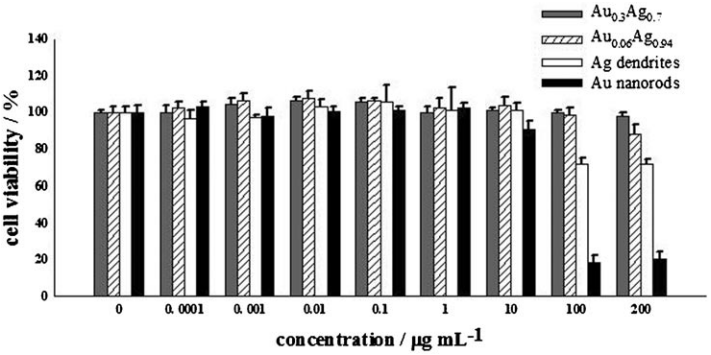

Figure 6. Biocompatibility of the Au nanorods, Ag dendrite particles, and Au_xAg_{1-x} nanostructured dendrites was analyzed by using a MTT assay. The malignant A549 cancer cells were treated with various dosages of nano-materials from 0.0001 $\mu g\,mL^{-1}$ to 200 $\mu g\,mL^{-1}$ with an incubation of 24 h.

cell viability from the MTT assay with Au nanorods, Ag dendrites, and hollow $Au_{0.06}Ag_{0.94}$ and $Au_{0.30}Ag_{0.70}$ dendrites. To eliminate unbound cetyltrimethylammonium bromide (CTAB) molecules, the Au nanorods were washed twice in de-ionized water prior to the cell viability experiments. The cells treated with Au nanorods show an apparent cell-viability dose dependence. The cell viability decreased as particle concentration increased, with viable cells dropping to 18% at 100 $\mu g\,mL^{-1}$ for Au nanorods. The toxicity in Au nanorods can be attributed to the presence of CTAB surfactants on the nanorod surfaces.[17] When treating cells with Ag dendrites, toxicity was observed at higher particle concentrations, with cell viability dropping to 71% at 100 $\mu g\,mL^{-1}$. It seems that the additional Au component in $Au_{0.06}Ag_{0.94}$ and $Au_{0.3}Ag_{0.7}$ dendrites gives rise to better biocompatibility. Dendrite $Au_{0.3}Ag_{0.7}$ shows especially good biocompatibility with cell viability of more than 95% for a particle concentration of up to 200 $\mu g\,mL^{-1}$, while $Au_{0.06}Ag_{0.94}$ shows a decreasing trend in cell viability to 88% at 200 $\mu g\,mL^{-1}$. The MTT assay demonstrated lower toxicity in hollow Au_xAg_{1-x} dendrites.

The performance of photothermal cancer therapy using Au_xAg_{1-x} dendrite nanoparticles and Au nanorods: As shown in the UV/Vis absorption spectra of Figure 5, the hollow $Au_{0.3}Ag_{0.7}$ dendrite nanomaterials have the strongest absorption in the NIR region. This suggests that the $Au_{0.3}Ag_{0.7}$ dendrites might act as efficient absorbers for destroying cancer cells if an NIR laser is used. Malignant lung cancer cells A549, which overexpress the epidermal growth factor receptor (EGFR) on the cell surfaces, were used to study the photothermal effect. By conjugating anti-EGFR monoclonal antibodies with $Au_{0.3}Ag_{0.7}$ dendrites, we can

evaluate the cancer cells killing efficiency. As there is a possible electrostatic interaction between the negatively charged $Au_{0.3}Ag_{0.7}$ dendrites (determined using zeta potential) and the positively charged segment of the anti-EGFR,[18] the $Au_{0.3}Ag_{0.7}$ dendrites can readily conjugate with anti-EGFR. The laser irradiation dosages were varied from 5 to 35 $W cm^{-2}$ with a focused spot of 1 mm^2 for 4 min. The concentration of $Au_{0.3}Ag_{0.7}$ dendrite particles was fixed at 150 $\mu g mL^{-1}$. After NIR laser treatment, the cells were incubated with calcein AM and ethidium homodimer-1 (EthD-1) to verify the cell viability by using fluorescence microscopy. The green fluorescence color of calcein AM displays the viable cells and the red fluorescence color of EthD-1 indicates the dead cells. As can be seen in Figure 7, the anti-EGFR conjugated with $Au_{0.3}Ag_{0.7}$ dendrites treated A549 cells shows a significant loss of viability, with the area lacking green fluorescence and exhibiting red fluorescence beginning at 15 $W cm^{-2}$. When the laser power dropped to 10 $W cm^{-2}$, no photothermal destruction was observed in A549 cells. For comparison, $Au_{0.06}Ag_{0.94}$ dendrites with lower absorption in the NIR region were also studied. When the A549 cells were exposed to the NIR laser after being treated with anti-EGFR-conjugated $Au_{0.06}Ag_{0.94}$ dendrites, only a slight destruction of A549 cells was observed, even when the laser power density was increased to 35 $W cm^{-2}$ (see Supporting Information Figure S2). It should be mentioned that our NIR laser's maximum power density is 35 $W cm^{-2}$ for a laser spot of 1 mm^2.

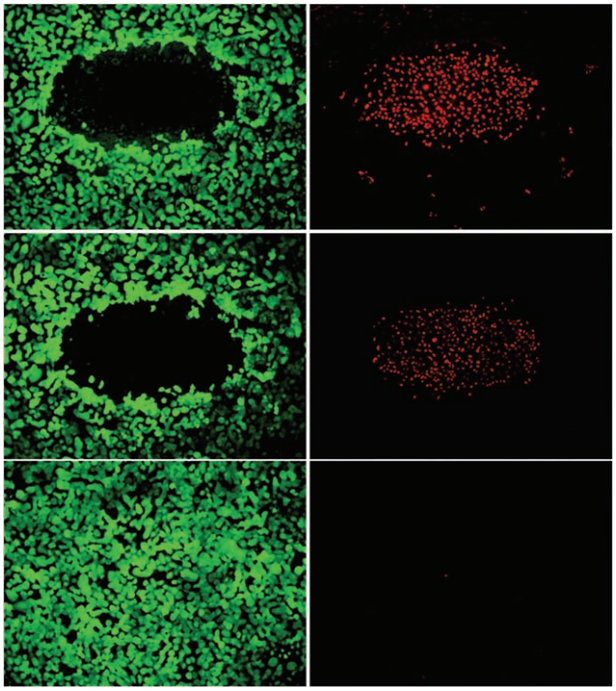

Figure 7. Anti-EGFR conjugated with $Au_{0.3}Ag_{0.7}$ dendrites (150 $\mu g mL^{-1}$) treated A549 cancer cells were irradiated by laser dosages of 20 $W cm^{-2}$ (top row), 15 $W cm^{-2}$ (middle row), and 10 $W cm^{-2}$ (bottom row) for 4 min. The left column shows staining by green fluorescence dye, calcein AM, for living cells. The right column displays stainning by EthD-1, in which the red fluorescence color indicates cell death.

The anti-EGFR conjugated with Au nanorods was also studied for the photoinduced thermal effect on A549 cancer cells. The Au nanorods were synthesized to exhibit an aspect ratio of four, giving them a maximum absorption band close to a wavelength of 800 nm. The Au nanorods were 36 nm in length and 8.8 nm in diameter (see Supporting Information Figure S3). The presence of CTAB gave the Au nanorods a positive surface charge. To conjugate with anti-EGFR, Au nanorods were altered to have a negative surface charge by coating them with poly(styrenesulfonate) (PSS), following the method from El-sayed et al.[7] The anti-EGFR conjugated with Au nanorods treated with A549 cancer cells were then irradiated for 4 min by NIR laser irradiation at various laser powers. The concentration of Au nanorods used for photoablation was raised to 500 $\mu g mL^{-1}$. We found that the required concentration for Au nanorods to give efficient photodestruction of A549 cells should be at least 450 $\mu g mL^{-1}$. As demonstrated in Figure 8, a significant loss of cancer cell viability appeared at the power density of 30 $W cm^{-2}$, at which a clear void in calcein AM staining and a red fluorescence spot in EthD-1 staining can be seen. However, no damage to A549 cancer cells was observed when the laser dosage was turned down to 25 $W cm^{-2}$. It is apparent that a higher particle concentration and a more in-

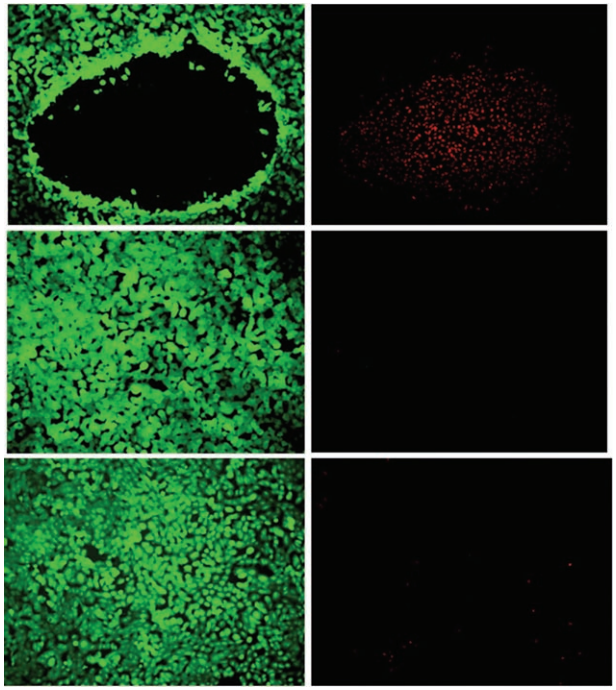

Figure 8. Anti-EGFR conjugated with Au nanorods (500 $\mu g mL^{-1}$) treated A549 cancer cells were irradiated by laser dosages of 30 $W cm^{-2}$ (top row), 25 $W cm^{-2}$ (middle row), and 20 $W cm^{-2}$ (bottom row) for 4 min. The left column shows staining by green fluorescence dye, calcein AM, for living cells. The right column displays stainning by EthD-1, in which the red fluorescence color indicates cell death.

tense laser power are required for the efficient photothermal damage of A549 cells using Au nanorods.

Figure 9 illustrates the cell viability versus NIR laser power for A549 cells treated with anti-EGFR conjugated with $Au_{0.3}Ag_{0.7}$ dendrites (500 μg mL^{-1}) and anti-EGFR conjugated with Au nanorods (500 μg mL^{-1}). The irradiated cells were stained with calcein AM immediately after NIR laser irradiation. The green fluorescence intensity of the observing area was integrated to quantify the A549-viable cells. The integrated green fluorescence light intensity was then divided by the fluorescence intensity of the control cells, producing cell viability (%). The control cells without treatment of the nanomaterials were irradiated by using the same NIR laser power under the same illumination conditions. A dramatic loss of viability appeared in the power range of 10–15 W cm^{-2} when the cells were treated with anti-EGFR conjugated with $Au_{0.3}Ag_{0.7}$ dendrites. On the other hand, cell viability exhibited a significant decrease until the laser power was increased to the range of 25–30 W cm^{-2} for Au nanorods. Once again, these results suggest that $Au_{0.3}Ag_{0.7}$ dendrites act as efficient photothermal absorbers for destroying cancer cells.

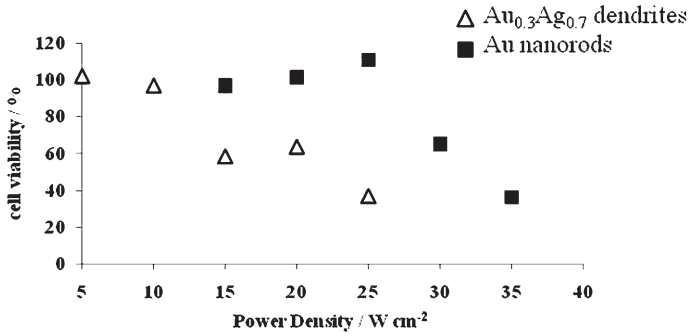

Figure 9. A549 cell viability versus the power density of the NIR laser; (△) A549 cells treated with anti-EGFR conjugated with $Au_{0.3}Ag_{0.7}$ nanostructured dendrites and (■) A549 cells treated with anti-EGFR conjugated with Au nanorods.

The lower particle concentration and lower NIR laser power for $Au_{0.3}Ag_{0.7}$ nanostructured dendrites, compared to those for Au nanorods, for the photodestruction of cancer cells may be attributed to the following reasons. First, the Au nanorods were synthesized in the presence of CTAB as a capping agent, and further modified by PSS to conjugate with anti-EGFR. Thus, the surface framework may have affected photon ($h\nu$) absorption, therefore reducing heat transfer to the surrounding cancer cells. As a result, a larger particle concentration and a higher NIR laser dosage were required for Au nanorods to induce sufficient heat for cancer cell destruction. The surface of the $Au_{0.3}Ag_{0.7}$ dendrite nanoparticles is surfactant-free and, hence, there is no hindrance to block absorption of photons and heat transfer from particles to the surrounding cancer cells. Therefore, photothermal cancer therapy can be achieved easily by using $Au_{0.3}Ag_{0.7}$ dendrites. The other contribution might be due to the large surface area of the hollow $Au_{0.30}Ag_{0.70}$ nanostructured dendrites, which provide more binding sites for anti-EGFR, leading to efficient selective targeting for photothermal destruction.

Conclusions

We have presented a new class of Au_xAg_{1-x} nanostructured dendrites with a hollow interior. The composition of Au/Ag ratio is tunable by adjusting the amount of added $HAuCl_4$ to the Ag dendrites solution. It was found that the resulting hollow $Au_{0.3}Ag_{0.7}$ dendrites exhibited strong NIR absorption and showed good biocompatibility. The NIR absorption band of $Au_{0.3}Ag_{0.7}$ dendrites allows them to serve as photothermal absorbers for photothermal therapy. By conjugating with anti-EGFR for specific binding on A549 lung cancer cells, the hollow $Au_{0.3}Ag_{0.7}$ dendrites used lower particle concentration and less laser power for cancer cell destruction relative to that needed with Au nanorods. The effective photothermal capability of hollow $Au_{0.3}Ag_{0.7}$ nanostructured dendrites is probably due to their surfactant-free surface and large surface area.

Experimental Section

Preparation of dendritic Ag nanostructures: The dendritic Ag nanostructures were synthesized by reducing Ag^+ ions with ascorbic acid (AsA). First, an aqueous solution of AsA (3 mL, 100 mM) was mixed with methanol (10 mL). Subsequently, of an aqueous solution of $AgNO_3$ (1 mL, 6 mM) was added to the solution of AsA solution in water/methanol (13 mL) and aged for 10 min at room temperature. The color changed from colorless to blackish. After aging, the products were collected by centrifugation to remove supernatants and were then washed for further analysis.

For the observation of the time-dependent TEM images, the aging solution at different time stages was pipetted onto a TEM mesh, covered with a filter paper to soak up the solvent for drying because of the short reaction period.

Preparation of core-free Au_xAg_{1-x} nanostructured dendrites: To synthesize core-free Au_xAg_{1-x} nanostructured dendrites, the as-prepared dendritic Ag nanostructures (14 mL) were collected and washed with water, then re-dispersed into water (3 mL) that contained poly(vinylpyrrolidone) (PVP) (MW: 55000) polymer (0.33 mM). Subsequently, various amounts of an aqueous solution of $HAuCl_4$ (1 mM; 0.8 mL, 0.75 mL, 0.5 mL, 0.25 mL, and 0.125 mL) were carefully dripped into the PVP-containing Ag dendritic solution. Magnetic stirring was employed for a reaction of 6 h. After the hollowing reaction, the final products were collected by centrifugation. A saturated aqueous solution of NaCl was then used to wash the hollowing products to remove AgCl byproducts. These purification steps were repeated several times.

Preparation of Au nanorods with an aspect ratio of four: The Au nanorods were prepared by using the seedless growth method in aqueous solution following a previous report.[19] Cetyltrimethylammonium bromide (CTAB) was used as a capping agent. In a typical synthesis, an aqueous solution containing CTAB (5 mL, 0.1 M) and $HAuCl_4$ (0.5 mM) was prepared. Next, an aqueous solution of $AgNO_3$ solution was added. The Au^{III} was reduced to Au^{I} by adding of an aqueous solution of ascorbic acid (30 μL, 0.1 M) under vigorous stirring. Nucleation and growth were initiated by quickly injecting of an aqueous $NaBH_4$ solution (2 μL, 1.6 mM) under vigorous stirring.

Preparation of anti-EGFR conjugated with Au nanorods and anti-EGFR conjugated with Au_xAg_{1-x} dendrites: Because of the surface capping by CTAB, the surface charge of the Au nanorods was positive. To conjugate the nanorods with anti-EGFR, the surface charge of Au nanorods was altered to be negative by coating them with poly(styrenesulfonate) (PSS) polyelectrolytes.[7,20] The Au nanorods were mixed with PSS in aqueous solution of NaCl (1 mM) in a volume ratio of 10:1. The reaction was allowed to proceed for 30 min. Then, the solution was purified using the centrifugation/resuspension process to remove unbound PSS. After modification of the surface with PSS, the nanorods were redispersed in *N*-(2-hydroxyethyl)piperazine-*N*′-2-ethanesulfonic acid (HEPES) solution (pH 7.4), and then mixed with anti-EGFR for 20 min. The anti-EGFR antibodies can bind to PSS-coated Au nanorods through electrostatic interactions.[7] The Au nanorods conjugated with anti-EGFR were centrifuged and redispersed into phosphate-buffered saline (PBS, pH 7.4). The hollow Au_xAg_{1-x} dendritic nanostructures conjugated with anti-EGFR were prepared by incubating with anti-EGFR in HEPES buffer solution for 30 min. After conjugating with anti-EGFR, the Au_xAg_{1-x} dendrites were then centrifuged and redispersed in PBS buffer solution to form a stable stock solution at 4 °C for several days.

Evaluation the biocompatibility of Au_xAg_{1-x} and Ag dendrites and Au nanorods: The A549 cells were cultured in a 96-well microplate with Dulbecco's modification of Eagle's medium (DMEM, cellgro) plus 5% fetal bovine serum (FBS, Gem Cell) in an initial density of 5×10^3 cells per well. They were maintained at 37 °C in a humidified atmosphere of 95% air and 5% CO_2. After 48 h, serial dilutions of nanomaterials, that is, Au_xAg_{1-x} dendrites, Ag dendrites, and Au nanorods, with particle concentrations of 0.0001, 0.001, 0.01, 0.1, 1, 10, 100, and 200 $\mu g\,mL^{-1}$ were added to the culture wells to replace the original culture medium, with a final volume of 100 μL. Following one day of continuous exposure to the nanomaterials, cell viability was determined using the 3-(4,5-dimethylthiazol-2-yl)-2,5-diphenyltetrazolium bromide (MTT) assay.[21] In this assay, cells that properly metabolize the MTT dye undergo a visible color change, while cells that are incapable of metabolizing the dye remain colorless. The culture medium was removed and replaced by 100 μL of the new culture medium containing 10% MTT reagent. The cells were then incubated for 4 h at 37 °C to allow the formation of formazan dye. The medium containing 10% MTT reagent was replaced by DMSO, which was used to solubilize the formazan crystals. After aging for 10 min followed by centrifugation for 10 min, 80 μL from each well was transferred to a new plate for spectrophotometric measurements. The quantification of cell viability was performed using optical absorbance (540/690 nm) and an ELISA plate reader.

NIR photothermal experiments: Malignant lung cells A549, which overexpress EGFR on the cell surface, were cultured in 96-well plates with Dulbecco's modification of Eagle's medium (DMEM, cellgro) plus 5% fetal bovine serum (FBS, Gem Cell) at 37 °C under 5% CO_2 until fully confluent. Each well contained 1×10^5 cells. The NIR-induced thermal therapy experiments were performed by using a diode continuous-wave (CW) laser with an irradiation wavelength of 808 nm. After incubation of anti-EGFR-conjugated nanomaterials with A549 cancer cells for 45 min, the DMEM medium was removed, then rinsed with PBS buffer solution three times to remove unbound or non-specific bound anti-EGFR-conjugated nanomaterials from the surface of A549 lung cancer cells. The A549 cancer cells were immersed in fresh medium prior to irradiation by the diode CW laser. The efficiency of photoinduced cancer cell thermal ablation was investigated with various concentrations of anti-EGFR-conjugated nanomaterials and different power densities of the CW laser at 808 nm. Each well was exposed to the laser light with a focused area of 1 mm^2 for 4 min. The cell viability was confirmed by staining the cells with calcein AM and ethidium homodimer-1 (EthD-1), for which green fluorescence from calcein AM indicated live cells and red fluorescence from EthD-1 indicated dead cells.

Characterization: Electron micrographs were obtained using transmission electron microscopes (JEOL 3010 at 300 KV and PHILIPS CM-200 at 200 KV). A drop of the sample was placed on a copper mesh coated with an amorphous carbon film, followed by evaporation of the solvent in a vacuum desiccator. Scanning electron microscopy (SEM) images of the as-synthesized nanomaterials on the silicon substrates were obtained on a field-emission scanning electron microscope (XL-40FEG; Philips Research Europe, Eindhoven, The Netherlands). For the EDX measurements, both dendritic Ag particles and core-free Au_xAg_{1-x} dendrites were deposited on the silicon substrates without platinum coating. The crystalline structures were identified using an X-ray diffractometer (XRD-7000S; Shimadzu Corporation, Tokyo, Japan) with $Cu_{K\alpha}$ radiation ($\lambda=$ 1.54060 Å) at 30 kV and 30 mA. A UV/Vis spectrophotometer (Hewlett–Packard 8452 A) was used to characterize the optical absorption.

Acknowledgements

We would like to thank the National Science Council of Taiwan for financially supporting this work.

[1] a) J. L. West, N. J. Halas, *Annu. Rev. Biomed. Eng.* **2003**, *5*, 285–292; b) G. F. Paciotti, L. Myer, D. Weinreich, D. Goia, N. Pavel, R. E. McLaughlin, L. Tamarkin, *Drug Delivery* **2004**, *11*, 169–183; c) K. K. Jain, *Technol. Cancer Res. Treat.* **2005**, *4*, 407–416.

[2] a) X. Wu, H. Liu, J. Liu, K. N. Haley, J. A. Treadway, J. P. Larson, N. Ge, F. Peale, M. P. Bruchez, *Nat. Biotechnol.* **2003**, *21*, 41–46; b) W. C. W. Chan, D. J. Maxwell, X. Gao, R. E. Bailey, M. Han, S. Nie, *Curr. Opin. Biotechnol.* **2002**, *13*, 40–46; c) A. P. Alivisatos, *Nat. Biotechnol.* **2004**, *22*, 47–52; d) K. Sokolov, J. Aaron, B. Hsu, D. Nida, A. Gillanwater, M. Follen, C. Macaulay, K. Adler-Storthz, B. Korgel, M. Discour, R. Pasqualini, W. Arap, W. Lam, R. Richartz-Kortum, *Technol. Cancer Res. Treat.* **2003**, *2*, 491–504.

[3] a) L. R. Hirsch, R. J. Stafford, J. A. Bankson, S. R. Sershen, B. Rivera, R. E. Rrice, J. D. Hazle, N. J. Halas, J. L. West, *Proc. Natl. Acad. Sci. USA* **2003**, *100*, 13549–13554; b) C. Loo, A. Lowery, N. Halas, J. West, R. Drezek, *Nano Lett.* **2005**, *5*, 709–711; c) D. P. O'Neal, L. R. Hirsch, N. J. Halas, J. D. Payne, J. L. West, *Cancer Lett.* **2004**, *209*, 171–176.

[4] V. P. Zharov, E. N. Galitovskaya, C. Johnson, T. Kelly, *Laser Surg. Med.* **2005**, *37*, 219–226.

[5] J. Chen, D. Wang, J. Xi, L. Au, A. Siekkinen, A. Warsen, Z. Y. Li, H. Zhang, Y. Xia, X. Li, *Nano Lett.* **2007**, *7*, 1318–1322.

[6] J. Kim, S. Park, J. E. Lee, S. M. Jin, J. H. Lee, I. S. Lee, I. Yang, J. S. Kim, S. K. Kim, M. H. Cho, T. Hyeon, *Angew. Chem.* **2006**, *118*, 7918–7922; *Angew. Chem. Int. Ed.* **2006**, *45*, 7754–7758.

[7] X. Huang, I. H. El-Sayed, W. Qian, M. A. El-Sayed, *J. Am. Chem. Soc.* **2006**, *128*, 2115–2120.

[8] M. H. Rashid, T. K. Mandal, *J. Phys. Chem. C* **2007**, *111*, 16750–16760.

[9] a) X. Wen, Y.-T. Xie, M. W. C. Mark, K. Y. Cheung, X.-Y. Li, R. Renneberg, S. Yang, *Langmuir* **2006**, *22*, 4836–4842; b) L. Lu, A. Kobayashi, Y. Kikkawa, K. Tawa, Y. Ozaki, *J. Phys. Chem. B* **2006**, *110*, 23234–23241.

[10] a) J. Fang, H. You, P. Kong, Y. Yi, X. Song, B. Ding, *Cryst. Growth Des.* **2007**, *7*, 864–867; b) J. Yang, L. Qi, D. Zhang, J. Ma, H. Cheng, *Cryst. Growth Des.* **2004**, *4*, 1371–1375; c) W. Shizhong, X. Houwen, *J. Phys. Chem. B* **2000**, *104*, 5681–5685; d) X. Sun, M. Hagner, *Langmuir* **2007**, *23*, 9147–9150.

[11] a) G.-J. Lee, S.-I. Shin, S.-G. Oh, *Chem. Lett.* **2004**, *33*, 118–119; b) W.-T. Wu, W. Pang, G. Xu, L. Shi, Q. Zhu, Y. Wang, F. Lu, *Nanotechnology* **2005**, *16*, 2048–2051.

[12] T. Fukuyo, H. Imai, *J. Cryst. Growth* **2002**, *241*, 193–199.

[13] F. Shi, Y. Song, J. Niu, X. Xia, Z. Wang, X. Zhang, *Chem. Mater.* **2006**, *18*, 1365–1368.

[14] a) T. A. Witten, L. M. Sander, *Phys. Rev. Lett.* **1981**, *47*, 1400–1403; b) S. R. Forrest, T. A. Witten, *J. Phys. A* **1979**, *12*, L109–L117; c) P. Meakin, *Phys. Rev. Lett.* **1983**, *51*, 1119–1122.

[15] a) Y. Sun, Y. Xia, *Science* **2002**, *298*, 2176–2179; b) Y. Sun, Y. Xia, *J. Am. Chem. Soc.* **2004**, *126*, 3892; c) Y. Sun, B. T. Mayers, Y. Xia, *Nano Lett.* **2002**, *2*, 481–485.

[16] Y.-N. Tan, J. Y. Lee, D. I. C. Wang, *J. Phys. Chem. C* **2007**, *111*, 14084–14090.
[17] a) H. Takahashi, Y. Niidome, T. Niidome, K. Kaneko, H. Kawasaki, S. Yamada, *Langmuir* **2006**, *22*, 2–5; b) E. E. Connor, J. Mwamuka, A. Gole, C. J. Murphy, M. D. Wyatt, *Small* **2005**, *1*, 325–327; c) H. Ding, K. T. Yong, I. Roy, H. E. Pudavar, W. C. Law, E. J. Bergey, P. N. Prasad, *J. Phys. Chem. C* **2007**, *111*, 12552–12557.
[18] a) C. J. Ackerson, P. D. Jadzinsky, G. J. Jensen, R. D. Kornberg, *J. Am. Chem. Soc.* **2006**, *128*, 2635–2640; b) M. A. Hayat, *Colloidal Gold: Principles, Methods, and Applications*, Academic Press, San Diego, CA, **1989**.
[19] P. Zijlstra, C. Bullen, J. W. M. Chon, M. Gu, *J. Phys. Chem. B* **2006**, *110*, 19315–19318.
[20] D. I. Gittins, F. Caruso, *J. Phys. Chem. B* **2001**, *105*, 6846–6852.
[21] J. Carmichael, W. G. DeGraff, A. F. Gazdar, J. D. Minna, J. B. Mitchell, *Cancer Res.* **1987**, *47*, 936–942.

Received: January 21, 2008
Published online: March 11, 2008

